Self-excited oscillation and synchronization of an on-fiber optomechanical cavity

Eyal Buks⬥

Andrew and Erna Viterbi Department of Electrical Engineering, Technion, Haifa 32000, Israel

Ivar Martin

Materials Science Division, Argonne National Laboratory, Argonne, Illinois 60439, USA

We study a fully on-fiber optomechanical cavity and characterize its performance as a sensor. The cavity is formed by patterning a suspended metallic mirror near the tip of an optical fiber and by introducing a static reflector inside the fiber. Optically induced self-excited oscillation (SEO) is observed above a threshold value of the injected laser power. The SEO phase can be synchronized by periodically modulating the optical power that is injected into the cavity. Noise properties of the system in the region of synchronization are investigated. Moreover, the spectrum is measured near different values of the modulation frequency, at which phase locking occurs. A universal behavior is revealed in the transition between the regions of phase locked and free running SEO.

I. INTRODUCTION

Resonant detection is a widely employed technique in a variety of applications. A detector belonging to this class typically consists of a resonator, which is characterized by an angular resonance frequency ω_0 and a characteristic damping rate γ_0. Detection is achieved by coupling a physical parameter of interest, denoted here as q, to the resonator in such a way that ω_0 becomes q-dependent. The sensitivity of the detection scheme that is employed for monitoring the parameter of interest q can be characterized by the minimum detectable change in q, denoted as δ_q. For small changes, δ_q is related to the minimum detectable *relative* change in the frequency $\sigma_\omega = \delta_{\omega_0}/\omega_0$ by the relation $\delta_q = |\partial\omega_0/\partial q|^{-1}\omega_0\sigma_\omega$. The dimensionless parameter σ_ω, in turn, typically depends on the noises affecting the resonator and on the averaging time t_a of the measurement.

A commonly employed detection scheme is based on externally driving the resonator with a monochromatic force at a frequency close to the resonance frequency and monitoring the response using homodyne detection of a displacement sensor signal. For this case, the normalized minimum detectable change in the frequency is found to be given by $\sigma_\omega = \sigma_{\omega 0}$, where [1]

$$\sigma_{\omega 0} = \left(\frac{2\gamma_0 k_\mathrm{B} T_\mathrm{eff}}{U_0 \omega_0^2 t_a}\right)^{1/2}, \tag{1}$$

where k_B is Boltzmann's constant, T_eff is the noise effective temperature (which is identical to the thermodynamic temperature in the absence of any other sources of noise), and U_0 is the energy stored in the externally driven resonator in steady state. Note that Eq. (1) is derived by assuming that the response of the resonator is linear and by assuming the classical limit, i.e., $k_\mathrm{B} T_\mathrm{eff} \gg \hbar\omega_0$, where $\hbar$ is Planck's constant. The generalization of Eq. (1) for the case of nonlinear response is discussed in Ref. [2]. Note that other contributions to σ_ω (e.g., instrumental noise) are not analyzed in this paper.

In the just mentioned scheme, the resonator is driven into a so-called state of forced oscillation (FO) by applying a fixed periodic external force. Alternatively, in some cases backreaction effects can be exploited for generating a so-called state of self-excited oscillation (SEO) [3–6]. In this paper, we study SEO in an on-fiber optomechanical cavity device (see Fig. 1), which is formed between a fiber Bragg grating (FBG) mirror, serving as a static reflector, and a vibrating mirror fabricated on a mechanical resonator next to the tip of the single-mode optical fiber. The movable mirror can be driven into the SEO state by injecting a monochromatic laser light into the fiber. The SEO occurs via bolometric feedback effects. Further, by periodically modulating the laser intensity, it is possible to lock the phase of SEO to a rational fraction of the modulation frequency.

Driving an on-fiber optomechanical cavity into the state of SEO is easier in comparison with the case of FO, which requires the fabrication of additional elements near the tip of the fiber that need to be electrically wired. In contrast, SEO can be induced by optical excitation only. In this paper, we study the performance of the device as a sensor in the regime of SEO, both with and without synchronization, and we compare the results to the case of FO [see Eq. (1)]. We find that synchronization gives rise to a suppression in phase noise, which in turn allows a sensitivity enhancement.

Optomechanical cavities [8–14] are widely employed for various sensing [3–6] and photonics [15–21] applications. Such systems may allow experimental study of the crossover between classical to quantum realms [22]. The effect of radiation pressure typically governs the optomechanical coupling (i.e., the coupling between the electromagnetic cavity and the mechanical resonator that serves as a movable mirror) when the finesse of the optical cavity is sufficiently high [10,12,23–26], whereas bolometric effects can contribute to the optomechanical coupling when optical absorption by the vibrating mirror is significant [11,27–34]. Generally, bolometric effects are dominant in systems comprised of relatively large mir-
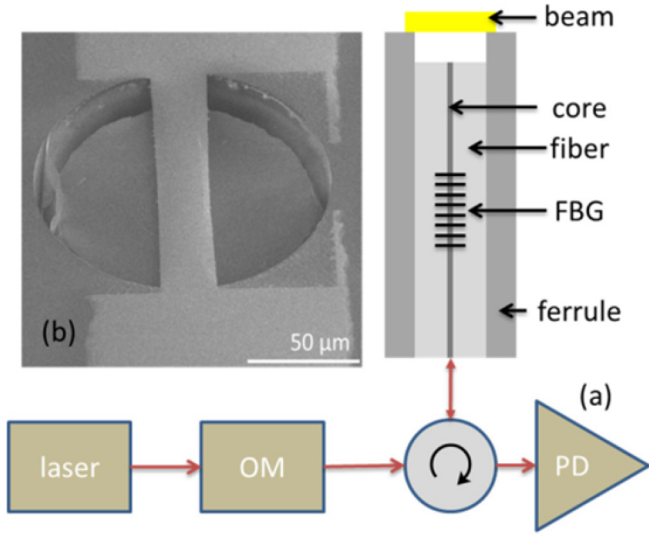
FIG. 1. Experimental setup. (a) A schematic drawing of the sample and the experimental setup. An on-fiber optomechanical cavity is excited by a tunable laser with an external Mach-Zehnder amplitude optical modulator (OM). The mechanical resonator has quality factor $\omega_0/2\gamma_0 = 3800$ and the cavity has finesse $\beta_F = 2.1$. The reflected light intensity is measured using a photodetector (PD), which is connected to an amplifier. (b) Electron micrograph of the suspended micromechanical mirror (reproduced from Ref. [7]), whose mass is $m = 1.1 \times 10^{-12}$ kg.

rors, in which the thermal relaxation rate is comparable to the mechanical resonance frequency [31–33,35]. These systems [11,27,29,35–37] exhibit many intriguing phenomena, including mode cooling [9,29,32,35,38–41], synchronization [42–44], and sidebands [45].

II. EXPERIMENTAL SETUP

The optomechanical cavity, which is schematically shown in Fig. 1(a), was fabricated on the flat polished tip of a single-mode fused silica optical fiber with an outer diameter of 126 μm (Corning SMF-28 operating at a wavelength band around 1550 nm) held in a zirconia ferrule [46]. A 10-nm-thick chromium layer and a 200 nm gold layer were successively deposited by thermal evaporation. The bilayer was directly patterned by a focused ion beam to the desired mirror shape (20-μm-wide doubly clamped beam). Finally, the mirror was released by etching approximately 12 μm of the underlying silica in 7% HF acid (90 min etch time at room temperature). The suspended mirror remained supported by the zirconia ferrule, which is resistant to HF.

The static mirror of the optomechanical cavity was provided by a FBG mirror [36] (made using a standard phase mask technique [47], with a grating period of 0.527 μm and length ≈ 8 mm) having a reflectivity band of 0.4 nm full width at half-maximum centered at $\lambda_0 = 1545$ nm. The length of the optical cavity was $l \approx 10$ mm, providing a free spectral range of $\Delta\lambda = \lambda_0^2/2n_{\text{eff}}l \approx 80$ pm (where $n_{\text{eff}} = 1.468$ is the effective refraction index for SMF-28).

Monochromatic light was injected into the fiber bearing the cavity on its tip from a laser source with an adjustable output

wavelength λ and power level P_L. The laser was connected through an optical circulator, which allowed the measurement of the reflected light intensity P_R by a fast responding photodetector [see Fig. 1(a)]. The detected signal was analyzed by an oscilloscope and a spectrum analyzer. The experiments were performed in vacuum (at residual pressure below 0.01 Pa) at a base temperature of 77 K. Thermal contraction gives rise to cooling-induced enhancement of the quality factor of the mechanical resonator [48]. In addition, cooling down using liquid nitrogen greatly improves the stability of temperature and allows the pressure to be maintained in the experimental chamber low without continuously applying active pumping. Further details on the device fabrication and the experimental setup can be found in Ref. [7].

The optically induced SEO in our device is attributed to the bolometric optomechanical coupling between the optical mode and the mechanical resonator [36,37]. While the phase of SEO randomly diffuses in time when the laser power that is injected into the cavity is kept constant, phase-locking [49–54] may occur when the laser power is periodically modulated in time. Such locking results in entrainment [55], i.e., synchronization [56,57] between the SEO and the external modulation [58].

III. EVOLUTION EQUATION

In the limit of small displacement, the rotating-wave approximation can be employed in order to derive a first-order evolution equation given by [37,59]

$$\dot{A} + (\Gamma_{\text{eff}} + i\Omega_{\text{eff}})A = \xi(t) + \vartheta(t). \tag{2}$$

The mechanical displacement is related to the complex amplitude A as $x(t) = x_0 + 2\,\text{Re}A(t)$, where x_0 is an optically induced static displacement. An overdot denotes a derivative with respect to time t. To lowest nonvanishing order in $|A|^2$, the damping rate Γ_{eff} and the angular resonance frequency Ω_{eff} are given by $\Gamma_{\text{eff}} = \Gamma_0 + \Gamma_2|A|^2$ and $\Omega_{\text{eff}} = \Omega_0 + \Omega_2|A|^2$. The term $\xi(t)$ represents the effective force that is generated due to the laser power modulation. The fluctuating term $\vartheta(t) = \vartheta_x(t) + i\vartheta_y(t)$, where both ϑ_x and ϑ_y are real, represents white noise [60,61], and the following is assumed to hold: $\langle\vartheta_x(t)\vartheta_x(t')\rangle = \langle\vartheta_y(t)\vartheta_y(t')\rangle = 2\Theta\delta(t - t')$ and $\langle\vartheta_x(t)\vartheta_y(t')\rangle = 0$, where $\Theta = \gamma_0 k_B T_{\text{eff}}/4m\omega_0^2$, γ_0 and ω_0 are, respectively, the intrinsic damping rate and angular frequency of the resonator, m is its mass, k_B is Boltzmann's constant, and T_{eff} is the effective noise temperature. Expressions for the coefficients x_0, Γ_0, Γ_2, Ω_0, and Ω_2, which all depend on the properties of the optical cavity and on the laser wavelength and power, are given in Appendix A. Both rates ω_0 and γ_0 are experimentally extracted from the line shape of the peak in the spectrum generated by thermal noise (see Fig. 6 of Ref. [36]).

IV. RESONANCE DETECTION WITH SEO

In the absence of laser modulation, i.e., when $\xi(t) = 0$, the equation of motion (2) describes a van der Pol oscillator [50]. Consider the case in which $\Gamma_2 > 0$, for which a supercritical Hopf bifurcation occurs when the linear damping coefficient Γ_0 vanishes. Above threshold, i.e., when Γ_0 becomes

negative, the amplitude A_r of SEO is given by $r_0 = \sqrt{-\Gamma_0/\Gamma_2}$ and the angular frequency Ω_H of SEO by $\Omega_H = \Omega_{\text{eff}}(r_0)$.

The method of resonance detection can be implemented in the regime of SEO. The normalized minimum detectable change in the frequency σ_ω in this regime has been evaluated in [7], and it was found to be given by

$$\sigma_\omega = \sigma_{\omega 0}\left(1 + \frac{\zeta_0^2}{4|\Gamma_0|\Gamma_2}\right)^{1/2}, \tag{3}$$

where $\zeta_0 = d\Omega_{\text{eff}}/d|A|$. The above result (3) indicates that for the same value of the stored energy U_0, the smallest detectable change δ_q in the measured parameter q is $(1 + \zeta_0^2/4|\Gamma_0|\Gamma_2)^{1/2}$ larger for the current case of SEO in comparison with the case of FO [see Eq. (1)]. The reduced sensitivity is attributed to the dependence of Ω_{eff} on the amplitude $|A|$ of oscillation, which gives rise to elevated phase noise. Recall that in the regime of SEO, in which no periodic driving is applied, the phase of oscillation is not externally dictated, and consequently it becomes more susceptible to noise. For the device under study in this work, the degradation factor is given by $(1 + \zeta_0^2/4|\Gamma_0|\Gamma_2)^{1/2} \simeq 10$.

V. SYNCHRONIZATION

In the regime of SEO, phase noise can be suppressed by modulating the injected laser power at an angular frequency ω_d close to the angular frequency Ω_{eff}. When fluctuations are dominated by phase noise, Eq. (2) can be simplified by disregarding fluctuations in the amplitude $|A|$ (i.e., by assuming that $|A| = r_0$). In this approach, one finds that the relative phase γ between mechanical oscillation and the applied modulation evolves in time according to [see Eq. (B11)]

$$\frac{d\gamma}{d\tau} + \sin\gamma = i_b + i_n, \tag{4}$$

where $i_b = (\omega_d - \Omega_{\text{eff}})/\omega_a$ is a normalized detuning, $\tau = \omega_a t$ is a dimensionless time variable, and ω_a is the modulation amplitude. The term i_n represents white noise having a vanishing expectation value $\langle i_n \rangle = 0$ and autocorrelation function $\langle i_n(\tau)i_n(\tau')\rangle = 2\gamma_g\delta(\tau - \tau')$, where $\gamma_g = \Theta/(\omega_a r_0^2)$ [see Eq. (B13)].

In the region of synchronization, in which $|i_b| \leqslant 1$, Eq. (4) has a stationary solution given by $\gamma = \sin^{-1} i_b$, whereas γ becomes time-dependent when $|i_b| > 1$. In that region and when noise is disregarded, the time evolution of $\gamma(\tau)$, which is given by Eq. (B15), is a periodic function of τ with a period given by $T_J = 2\pi/\sqrt{i_b^2 - 1}$ [see Eq. (B16)]. The Fourier series expansion of $d\gamma/d\tau$ is given by Eqs. (B24) and (B25). The periodic time evolution of the relative phase γ gives rise to sidebands in the spectrum at the angular frequencies $\omega_d + n\omega_s$, where n is an integer and the sideband spacing ω_s is given by $\omega_s = 2\pi\omega_a/T_J = \sqrt{(\omega_d - \Omega_{\text{eff}})^2 - \omega_a^2}$.

The equation of motion (4) indicates that the dynamics of the relative phase γ is governed by a potential $U_b(\gamma) = -\cos\gamma - i_b\gamma$ having the shape of a tilted washboard. The shape of the barriers separating local minima points of $U_b(\gamma)$ (when $|i_b| < 1$) can be controlled by adjusting the frequency detuning $\omega_d - \Omega_{\text{eff}}$ and modulation amplitude ω_a. The highly nonlinear response of the system near the onset point of syn-
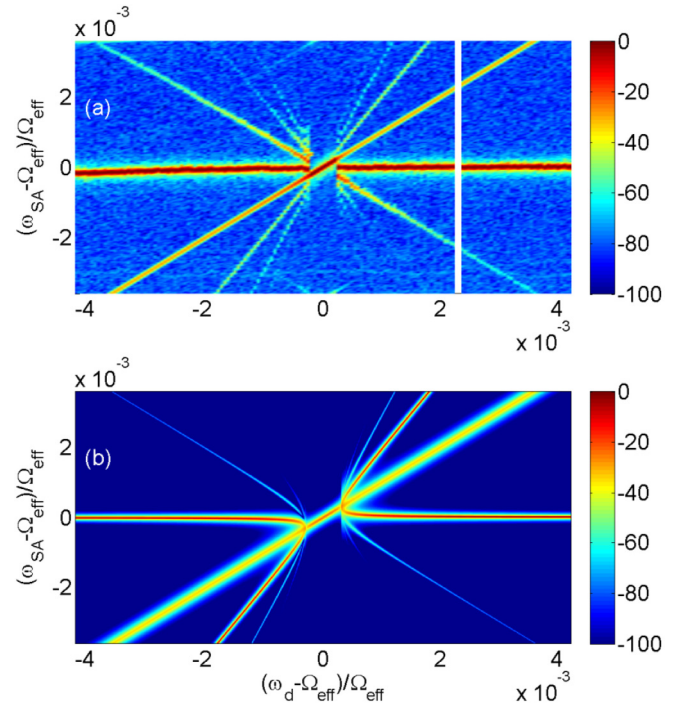
FIG. 2. Power spectrum vs detuning. (a) The measured power spectrum as a function of $(\omega_d - \Omega_{\text{eff}})/\Omega_{\text{eff}}$, where $\Omega_{\text{eff}}/2\pi = 236.4$ kHz. In this measurement, the average laser power is set to $P_L = 12$ mW (the SEO threshold power is 8.5 mW), the wavelength to $\lambda = 1545.498$ nm (10 pm red detuned from a cavity optical resonance), and the dimensionless laser modulation amplitude to 0.025. (b) Theoretical calculation of the power spectrum based on the solution of Eq. (4). In both plots, synchronization occurs when $|i_b| < 1$ and sidebands are observed when $|i_b| > 1$.

chronization can be exploited for some sensing applications. Note that an equation of motion similar to (4) governs the dynamics of a current-biased Josephson junction in the so-called overdamped regime [62]. The effect of the noise term i_n on voltage fluctuations across a Josephson junction in the quantum regime has been investigated in [63,64].

VI. SA MEASUREMENTS

The measured power spectrum of the photodetector signal is plotted in Fig. 2(a) as a function of $(\omega_d - \Omega_{\text{eff}})/\Omega_{\text{eff}} = i_b\omega_a/\Omega_{\text{eff}}$. In the absence of power laser modulation, the frequency of SEO is given by $\Omega_{\text{eff}}/2\pi = 236.4$ kHz. As can be seen from Fig. 2(a), in the region $|(\omega_d - \Omega_{\text{eff}})/\Omega_{\text{eff}}| \leqslant 2.1 \times 10^{-4}$ synchronization occurs, and thus $\omega_a/2\pi = 49.6$ Hz for this measurement. The above-discussed sidebands are clearly visible in the region $|(\omega_d - \Omega_{\text{eff}})/\Omega_{\text{eff}}| > \omega_a/\Omega_{\text{eff}}$, i.e., when $|i_b| > 1$. The theoretically calculated power spectrum is presented in Fig. 2(b) for comparison. The amplitudes of the sidebands are determined using the Fourier series expansion [see Eqs. (B24) and (B25)]. Good agreement between data and theory is found.

For the data presented in Fig. 2(a), synchronization occurs when $\omega_d/\Omega_{\text{eff}} \simeq 1$. Similar synchronization is observed when the ratio $\omega_d/\Omega_{\text{eff}}$ is tuned close to other rational values [42,43]. As an example, the measured power
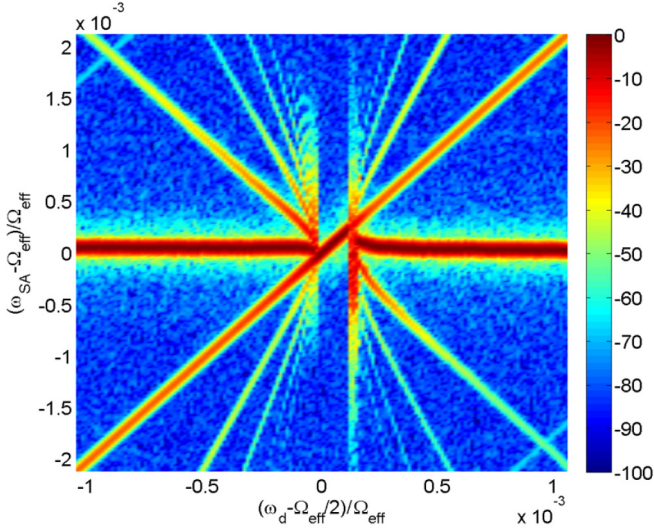
FIG. 3. Measured power spectrum vs detuning for the case in which $\omega_d/\Omega_{\mathrm{eff}} \simeq 1/2$. Other experimental parameters are listed in the caption of Fig. 2.

FIG. 4. The variance of the phase γ. (a) Normalized variance V_γ/γ_g as a function of i_b. The theoretical value is based on the integrated power spectrum of γ given by Eq. (7). In the numerical integration, the noise term i_n in a given time interval of length τ_s is represented by a random variable having a vanishing expectation value and a variance given by $2\gamma_g/\tau_s$. (b) The measured (crosses) and calculated (solid line) variance V_γ for the case $i_b = 0$ as a function of the normalized modulation amplitude γ_g^{-1}.

spectrum for the case in which $\omega_d/\Omega_{\mathrm{eff}} \simeq 1/2$ is shown in Fig. 3. As can be seen from the comparison with Fig. 2(a), the results are qualitatively similar. Although it is not shown here, very similar behaviors were also observed experimentally at other ratios, including $\omega_d/\Omega_{\mathrm{eff}} \simeq$ 1/3, 2/3, 1/4, 3/4, 1/5, 2/5, 3/5, and 4/5. This highlights universal aspects of the phase-locking phenomenon when the drive frequency approximately matches a rational multiple of the natural self-oscillation frequency.

Phase-locking near rational values of the ratio $\omega_d/\Omega_{\mathrm{eff}}$ is qualitatively discussed in Appendix C. It is found that just outside the locking regime, the frequency of oscillation undergoes a transition from a value dictated by the externally applied modulation to the value corresponding to free running SEO. Moreover, this transition is expected to obey a "square-root law" [65] for both integer and fractional values of the ratio $\omega_d/\Omega_{\mathrm{eff}}$. That is, the unlocking occurs continuously, with the deviation between the oscillator frequency from the (fraction of) drive frequency depending on the control parameter δ (drive amplitude, or detuning) as $\propto \sqrt{|\delta - \delta_c|}$, where δ_c is the critical—"unlocking"—value of δ. This universality in the behavior just outside the locking regime is demonstrated by the similarity of the spectrum measured near different locking regions (see Figs. 2 and 3).

VII. RESONANCE DETECTION IN THE REGION OF SYNCHRONIZATION

The effect of noise can be taken into account by linearizing Eq. (4), which becomes

$$\frac{d\gamma_n}{d\tau} + \gamma_n \cos\gamma = i_n, \tag{5}$$

where γ represents a solution in the noiseless case and γ_n is a fluctuating term added to γ due to noise. For the case $|i_b| < 1$, one finds from the stationary solution of Eq. (4) that $\cos\gamma = \sqrt{1 - i_b^2}$. The power spectrum $S_\gamma(w)$ of γ_n as a function of the

dimensionless angular frequency w can be found using Eq. (5) and the autocorrelation function $\langle i_n(\tau)i_n(\tau')\rangle$

$$S_\gamma(w) = \frac{\gamma_g}{\pi}\frac{1}{1 - i_b^2 + w^2}. \tag{6}$$

Near the synchronization threshold, i.e., when $|i_b| \lesssim 1$, noise may give rise to phase-slip events [i.e., transitions between neighboring wells of the tilted washboard potential $U_b(\gamma)$]. However, Eq. (6) has been derived by disregarding the contribution of these events. The validity of this approximation can be examined by numerically integrating the Langevin equation (4) and by extracting the variance of the phase γ, which is denoted by V_γ, from the result. The theoretical value is obtained from the integrated power spectrum given by Eq. (6),

$$\int_{-\infty}^{\infty} dw\, S_\gamma(w) = \frac{\gamma_g}{\sqrt{1 - i_b^2}}. \tag{7}$$

The plot in Fig. 4(a) shows a comparison between the numerically calculated value of the normalized variance V_γ/γ_g and the theoretically predicted value of $1/\sqrt{1 - i_b^2}$ that is obtained from Eq. (6).

The average rate of noise-induced phase slip events can be expressed using the Kramers formula in terms of the height V_b of the potential barrier localizing the metastable state [66,67]. With the help of the expansion $U_b = -i_b\pi/2 + (1 - i_b)\gamma_d - \gamma_d^3/6 + O(\gamma_d^4)$, where $\gamma = \pi/2 + \gamma_d$, one finds that near synchronization threshold the barrier height is given by $V_b = (4\sqrt{2}/3)(1 - i_b)^{3/2}$. The escape rate predicted by Kramers is proportional to the Arrhenius factor given by $\exp(-V_b/\gamma_g)$. For the parameters of our experiment, this factor is negligibly small unless $1 - i_b \lesssim 10^{-8}$.

A measurement of the variance V_γ as a function of the modulation amplitude ω_a for the case of zero detuning (i.e., $i_b = 0$) is shown in Fig. 4(b). The variance is extracted from the PD signal using the method of zero crossing. The solid line indicates the theoretical prediction.

The correlation function $C_\gamma(\tau') = \langle \gamma_n(\tau + \tau') \gamma_n(\tau) \rangle$ can be determined using the Wiener-Khinchine theorem

$$C_\gamma(\tau') = \int_{-\infty}^{\infty} dw \, e^{iw\tau'} S_\gamma(w) = \frac{\gamma_g e^{-\sqrt{1-i_b^2}|\tau'|}}{\sqrt{1 - i_b^2}}, \quad (8)$$

and thus the following holds: $\langle \exp\{i[\gamma_n(\tau + \tau') - \gamma_n(\tau)]\}\rangle = 1 - \gamma_g|\tau'| + O(|\tau'|^2)$, i.e., the so-called jitter rate is given by γ_g. Note that γ_g is independent of i_b. In terms of the energy U_0 stored in the mechanical resonator, the dimensionful jitter rate is given by $\omega_a \gamma_g = (k_B T_{\text{eff}}/U_0)\gamma_0$. Note that the same jitter rate is obtained for the case of FO (provided that U_0 is unchanged).

In the region of synchronization, i.e., when $|i_b| < 1$, the resonance frequency Ω_{eff} can be determined by monitoring the relative phase γ. Consider an estimate of the averaged value of γ based on a sampling of the signal $\gamma + \gamma_n(\tau)$ over a sampling time of duration τ_a. The standard deviation δ_γ in this estimate is given by

$$\delta_\gamma = \left(\frac{2\pi S_\gamma(0)}{\tau_a}\right)^{1/2} = \left(\frac{2\gamma_g}{\tau_a(1 - i_b^2)}\right)^{1/2}. \quad (9)$$

The corresponding deviation δ_Ω in the estimated value of Ω_{eff} is given by $\delta_\Omega = \mathcal{R}\delta_\gamma$, where the responsivity $\mathcal{R}$ is given by $\mathcal{R} = (|d\gamma/d\Omega_{\text{eff}}|)^{-1} = \omega_a\sqrt{1 - i_b^2}$, and thus the normalized minimum detectable change in the frequency is given by $\delta_\Omega/\Omega_H = \sigma_{\omega 0}$, where $\sigma_{\omega 0}$ is given by Eq. (1). Thus for the same given stored energy U_0 in the mechanical resonator, the same sensitivity is expected in the regions of synchronization and FO. In other words, the above-discussed degradation in sensitivity occurring in the region of SEO [see Eq. (3)] can be fully eliminated by synchronization-induced suppression of phase noise. Similarly to the case of FO, in the regime of synchronization the phase of mechanical oscillation is externally dictated, and consequently noise is suppressed.

VIII. SUMMARY

In summary, the sensitivity of a detector based on a mechanical resonator is studied in the SEO regime. It is found that phase noise can be suppressed by externally applying a modulation. Moreover, the transition from the regions of synchronization and free running SEO is explored, and a universal behavior referred to as the square-root law is revealed.

ACKNOWLEDGMENTS

APPENDIX A: EVOLUTION EQUATION

The theoretical model [36,37] that is used to derive the evolution equation (2) is briefly described below. The micromechanical mirror in the optical cavity is treated as a mechanical resonator with a single degree of freedom x having mass m and linear damping rate γ_0 (when it is decoupled from the optical cavity). It is assumed that the angular resonance frequency of the mechanical resonator depends on the temperature T of the suspended mirror. For a small deviation of T from the base temperature T_0 (i.e., the temperature of the supporting substrate) it is taken to be given by $\omega_0 - \beta T_R$, where $T_R = T - T_0$ and where β is a constant. Furthermore, to model the effect of thermal deformation [29] it is assumed that a temperature-dependent force given by $m\theta T_R$, where θ is a constant, acts on the mechanical resonator [34]. When noise is disregarded, the equation of motion governing the dynamics of the mechanical resonator is taken to be given by

$$\frac{d^2x}{dt^2} + 2\gamma_0\frac{dx}{dt} + (\omega_0 - \beta T_R)^2 x = \theta T_R. \quad (A1)$$

The intracavity optical power incident on the suspended mirror is denoted by $P_L I(x)$, where P_L is the injected laser power, and the function $I(x)$ depends on the mechanical displacement x. The time evolution of the relative temperature T_R is governed by the thermal balance equation

$$\frac{dT_R}{dt} = Q - \kappa T_R, \quad (A2)$$

where $Q = \eta P_L I(x)$ is proportional to the heating power, η is the heating coefficient due to optical absorption, and κ is the thermal decay rate.

The function $I(x)$ depends on the properties of the optical cavity that is formed between the suspended mechanical mirror and the on-fiber static reflector. For sufficiently small x, the expansion $I(x) = I_0 + I_0'x + (1/2)I_0''x^2 + O(x^3)$ can be employed, where a prime denotes differentiation with respect to the displacement x. The coefficients I_0, I_0', and I_0'' are nearly periodic functions of the optical wavelength (see Fig. 2 of Ref. [7]).

Consider the case in which the laser power P_L is modulated in time according to $P_L(t) = P_0 + P_1(t)$, where P_0 is a constant and $P_1(t)$ is assumed to have a vanishing average. When both P_1 and $I - I_0$ are sufficiently small, the problem can be significantly simplified by employing the approximation $Q \simeq \eta P_0 I + \eta P_1 I_0$. The displacement $x(t)$ is expressed in terms of the complex amplitude A as $x(t) = x_0 + 2\text{Re}A$, where x_0, which is given by $x_0 = \eta\theta P_0 I_0/\kappa\omega_0^2$, is the averaged optically induced static displacement. For a small displacement, the evolution equation for the complex amplitude A is found to be given by Eq. (2) [37,42], where both the effective resonance frequency Ω_{eff} and the effective damping rate Γ_{eff} are real even functions of $|A|$. To second order in $|A|$ they are given by $\Gamma_{\text{eff}} = \Gamma_0 + \Gamma_2|A|^2$ and $\Omega_{\text{eff}} = \Omega_0 + \Omega_2|A|^2$, where $\Gamma_0 = \gamma_0 + \eta\theta P_0 I_0'/2\omega_0^2$, $\Gamma_2 = \gamma_2 + \eta\beta P_0 I_0''/4\omega_0$, γ_2 is the intrinsic mechanical nonlinear quadratic damping rate [68], $\Omega_0 = \omega_0 - \eta\beta P_0 I_0/\kappa$, and $\Omega_2 = -\eta\beta P_0 I_0''/\kappa$. Note that

the above expressions for Γ_{eff} and Ω_{eff} are obtained by making the following assumptions: $\kappa^2/\omega_0^3\lambda \ll \beta/\theta \ll 1/2\omega_0 x_0$ and $\kappa \ll \omega_0$, both of which typically hold experimentally [36]. For our experiment, the heating-induced frequency shift given by $\eta\beta P_0 I_0/\kappa$ is typically $\simeq 500$ Hz. The term $\xi(t)$ in Eq. (2) represents the thermal force that is generated due to the laser power modulation. For the case of a monochromatic modulation at angular frequency $\omega_{\text{d}} \simeq \Omega_{\text{eff}}$ it is given by $\xi(t) = \eta P_1 I_0 \theta \Omega_0^{-2} e^{-i\omega_{\text{d}}t}$.

APPENDIX B: MONOCHROMATIC MODULATION WITH $\omega_{\text{d}} \simeq \Omega_{\text{eff}}$

In cylindrical coordinates, the complex amplitude of mechanical oscillation A is expressed as $A = A_r e^{iA_\theta}$, where $A_r = \sqrt{A_x^2 + A_y^2}$ is positive, A_θ is real [69], and Eq. (2) is written as

$$\dot{A}_r + A_r \Gamma_{\text{eff}} = \xi_r + \vartheta_r \tag{B1}$$

and

$$\dot{A}_\theta + \Omega_{\text{eff}}(A_r) = \frac{\xi_\theta + \vartheta_\theta}{A_r}, \tag{B2}$$

where

$$\xi_r = \frac{A_x \xi_x + A_y \xi_y}{A_r}, \tag{B3}$$

$$\vartheta_r = \frac{A_x \vartheta_x + A_y \vartheta_y}{A_r}, \tag{B4}$$

$$\xi_\theta = \frac{A_x \xi_y - A_y \xi_x}{A_r}, \tag{B5}$$

$$\vartheta_\theta = \frac{A_x \vartheta_y - A_y \vartheta_x}{A_r}, \tag{B6}$$

$A = A_x + iA_y$, $\xi = \xi_x + i\xi_y$, where A_x, A_y, ξ_x, and ξ_y are all real, and the noise terms satisfy the following relations:

$$\langle \vartheta_r(t)\vartheta_r(t') \rangle = 2\Theta\delta(t - t'), \tag{B7}$$

$$\langle \vartheta_\theta(t)\vartheta_\theta(t') \rangle = 2\Theta\delta(t - t'), \tag{B8}$$

$$\langle \vartheta_r(t)\vartheta_\theta(t') \rangle = 0. \tag{B9}$$

Consider the case of a monochromatic modulation at angular frequency ω_{d}, which is assumed to be close to the angular frequency Ω_{eff}. When fluctuations in the amplitude A_r of SEO are disregarded, i.e., when it is assumed that $A_r = r_0$, Eq. (B2) becomes [see Eq. (B5)]

$$\dot{A}_\theta + \Omega_{\text{eff}} = -\omega_{\text{a}}\sin(A_\theta + \omega_{\text{d}}t) + \frac{\vartheta_\theta}{r_0}, \tag{B10}$$

where Ω_{eff} is treated as a constant and where ω_{a}, which is given by $\omega_{\text{a}} = \eta P_1 I_0 \theta/\Omega_0^2 r_0$, represents the modulation amplitude. In terms of the relative phase $\gamma = A_\theta + \omega_{\text{d}}t$ and the dimensionless time $\tau = \omega_{\text{a}}t$, Eq. (B10) can be rewritten as

$$\frac{d\gamma}{d\tau} + \sin\gamma = i_{\text{b}} + i_{\text{n}}, \tag{B11}$$

where

$$i_{\text{b}} = \frac{\omega_{\text{d}} - \Omega_{\text{eff}}}{\omega_{\text{a}}}, \tag{B12}$$

and where $i_{\text{n}} = \vartheta_\theta/(\omega_{\text{a}}r_0)$. With the help of Eq. (B8) one finds that

$$\langle i_{\text{n}}(\tau)i_{\text{n}}(\tau') \rangle = 2\gamma_{\text{g}}\delta(\tau - \tau'), \tag{B13}$$

where $\gamma_{\text{g}} = \Theta/(\omega_{\text{a}}r_0^2)$.

1. The noiseless case

Consider first the noiseless case, for which $i_{\text{n}} = 0$. Below the time evolution of γ in the region $|i_{\text{b}}| > 1$ is derived. Rewriting Eq. (B11) as $d\tau = d\gamma/(i_{\text{b}} - \sin\gamma)$ leads by integration to

$$\tau = \frac{2}{\sqrt{i_{\text{b}}^2 - 1}} \tan^{-1} \frac{i_{\text{b}}\tan\frac{\gamma}{2} - 1}{\sqrt{i_{\text{b}}^2 - 1}}. \tag{B14}$$

Inverting this relation yields

$$\gamma = 2\tan^{-1} \frac{1 + \sqrt{i_{\text{b}}^2 - 1}\tan\frac{\pi\tau}{T_{\text{J}}}}{i_{\text{b}}}, \tag{B15}$$

where the normalized period time T_{J} is given by

$$T_{\text{J}} = \frac{2\pi}{\sqrt{i_{\text{b}}^2 - 1}}, \tag{B16}$$

and thus

$$A_\theta = 2\tan^{-1} \frac{1 + \sqrt{i_{\text{b}}^2 - 1}\tan\left(\frac{\sqrt{i_{\text{b}}^2 - 1}\omega_{\text{a}}}{2\omega_{\text{d}}}\omega_{\text{d}}t\right)}{i_{\text{b}}} - \omega_{\text{d}}t. \tag{B17}$$

The averaged derivative $\langle d\gamma/d\tau \rangle$ is related to the period time T_{J} by

$$\left\langle \frac{d\gamma}{d\tau} \right\rangle = \frac{1}{T_{\text{J}}} \int_0^{T_{\text{J}}} \frac{d\gamma}{d\tau}d\tau = \frac{2\pi}{T_{\text{J}}}, \tag{B18}$$

thus [see Eqs. (B12) and (B16)]

$$\left\langle \frac{d\gamma}{d\tau} \right\rangle = \sqrt{i_{\text{b}}^2 - 1} \tag{B19}$$

and

$$-\left\langle \frac{dA_\theta}{dt} \right\rangle = \begin{cases} \omega_{\text{d}}, & |i_{\text{b}}| < 1, \\ \omega_{\text{d}} - \omega_{\text{a}}\sqrt{i_{\text{b}}^2 - 1}, & |i_{\text{b}}| \geqslant 1. \end{cases} \tag{B20}$$

Therefore, the signal $\cos A_\theta$ when $|i_{\text{b}}| \geqslant 1$ has a Fourier spectrum made of peaks at the angular frequencies $\omega_{\text{d}} + n\omega_{\text{s}}$, where n is an integer, and the sideband spacing ω_{s}, which is given by $\omega_{\text{s}} = 2\pi\omega_{\text{a}}/T_{\text{J}} = \sqrt{(\omega_{\text{d}} - \Omega_{\text{eff}})^2 - \omega_{\text{a}}^2}$ [see Eqs. (B12) and (B16)], depends on both the amplitude ω_{a} and frequency ω_{d} of the forcing term $\xi = r_0\omega_{\text{a}}A_r e^{-i\omega_{\text{d}}t}$.

2. Fourier expansion

With the help of Eqs. (B11), (B15), and (B16) together with the identity $\sin[2\tan^{-1}(s)] = 2s/(1 + s^2)$, one finds that

$$\frac{d\gamma}{d\tau} = \mathcal{V}\left(\frac{2\pi\tau}{T_{\text{J}}} + x_0\right), \tag{B21}$$

where the function $\mathcal{V}(x)$ is defined by

$$\mathcal{V}(x) = \frac{i_b^2 - 1}{i_b + \sin x}, \tag{B22}$$

and where

$$x_0 = \tan^{-1} \frac{1}{\sqrt{i_b^2 - 1}}. \tag{B23}$$

The Fourier expansion of the function $\mathcal{V}(x)$ is expressed as [see Eq. (B22)]

$$\mathcal{V}(x) = \sum_{k=-\infty}^{\infty} g_k e^{ikx}, \tag{B24}$$

where

$$g_k = \frac{i_b}{|i_b|} \sqrt{i_b^2 - 1} i^k \left(i_b - \frac{i_b}{|i_b|} \sqrt{i_b^2 - 1} \right)^{|k|}. \tag{B25}$$

Thus, the magnitude of the sideband peaks is relatively large when $|i_b| \gtrsim 1$. For $|i_b| \gg 1$, the sidebands become small and the relative phase becomes $\gamma \simeq (\omega_d - \Omega_{eff})t$ [see Eq. (B15)], i.e., the effect of laser modulation becomes weak.

APPENDIX C: SQUARE-ROOT LAW

In each of the regions of phase locking [51,52], the so-called winding number, which measures the oscillator phase accumulation relative to the phase of the drive, shows a plateau [53,70–72]. For concreteness, consider the region just outside the primary plateau where (for positive i_b) $0 < i_b - 1 \ll 1$, where i_b is the normalized detuning (recall that $|i_b| = 1$ at the onset of synchronization). The dimensionless frequency T_J^{-1} in this region is related to the critical parameter $i_b - 1$ by $T_J^{-1} \simeq 2^{-1/2} \pi^{-1} \sqrt{i_b - 1}$ [see Eq. (B16)]. As is shown in [65], a similar "square-root law" can be obtained for the region just outside any other plateau.

Consider a general 1D map having the form

$$\theta_{n+1} = \theta_n - \alpha + W_a \mathcal{F}(\theta_n), \tag{C1}$$

that describes, e.g., the phase of the oscillator motion observed every period of the applied drive. The detuning α is approximately $(\Omega_{eff} - \omega_d)2\pi/\omega_d$. W_a parametrizes the strength of applied periodic drive (zero in the absence of drive). The "map function" is a periodic real function, if we assume that the phase at the sampling step $n + 1$ only depends on the phase at step n, and the phases θ and $\theta + 2\pi$ are physically indistinguishable, $\mathcal{F}(\theta + 2\pi) = \mathcal{F}(\theta)$.

If the drive frequency is near the oscillator frequency, then the detuning is close to zero. The phase locking corresponds to a stable fixed point of the map, which can be found by solving the equation $\theta_{n+1} = \theta_n \equiv \theta^*$, that is,

$$\alpha = W_a \mathcal{F}(\theta^*), \tag{C2}$$

where θ^* is the stroboscopic value of the oscillator phase at the fixed point. Since the function $\mathcal{F}$ is continuous and periodic, it is bounded, and the fixed point of this map only exists for a small enough detuning.

Suppose now that the drive frequency is an integer fraction of the oscillator frequency, $\omega_d \approx \Omega_{eff}/p$. Then, since the
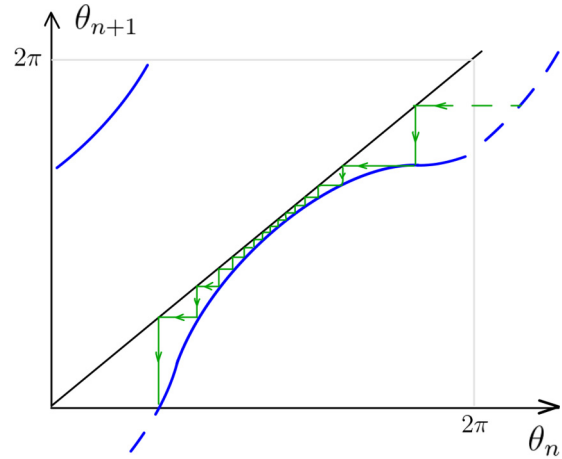
FIG. 5. Phase locking-unlocking transition. The blue line represents mapping of Eq. (C1) on the unlocked side of the transition. The green line is the staircase diagram that bounces between the map function and the diagonal $\theta_{n+1} = \theta_n$, graphically implementing the iteration procedure. Note that most of the iterations (longest time) is spend around the near-touching region. This leads to the "square-root" law for the splitting between the drive frequency and the oscillator frequency.

phase is defined modulo 2π, the effective detuning in this case is still small and the analysis of the locking transition is based on the same map equation. The locking will occur to $\Omega_{eff} = p\omega_d$. On the other hand, if the frequency of the drive is an integer multiple ($\omega_d \approx p\Omega_{eff}$) of the oscillator frequency, then during one period of the drive, the oscillator will only accrue a fraction $\approx 2\pi/p$ phase, which in general will correspond to too large of a detuning over a single period of the drive to allow for a fixed point solution. However, the problem can be reduced to a formally equivalent one by iterating the map p times,

$$\theta_{n+p} = \theta_n - p\alpha + \tilde{W}_a \tilde{\mathcal{F}}(\theta_n), \tag{C3}$$

where the effective detuning $p\alpha$ is now close to 2π, and the original treatment for the simple locking applies, with the resulting locked frequency being $\Omega_{eff} = \omega_d/p$. Note, however, that the amplitude and the form of the map function are now different, and generically smaller in magnitude that the $p = 1$ case. This makes locking to high-frequency drives in general less stable.

Now, let us look more carefully at the transition out of the locking regime as a function of detuning, α. Let us define α_c as the value of detuning and θ_c as the value of the fixed point θ^* at the transition between the locked and the running phase (unlocked) regimes, $\theta_c = \theta^*(\alpha_c)$. At the critical detuning, the slope of the map function $\mathcal{F}$ vanishes (see Fig. 5). We can expand the map function around this point up to second order,

$$\mathcal{F}(\theta) = \frac{\alpha_c}{W_a}[1 - z^2(\theta - \theta_c)^2] + O((\theta - \theta_c)^3), \tag{C4}$$

where z is a parameter that characterizes the curvature of the map function near θ_c. Indeed, as can be seen from Eq. (C1),

the map has a fixed point (i.e., a solution to the equation $\theta_{n+1} = \theta_n$) provided that $\alpha < \alpha_c$ (the fixed point is given by $\theta^* = \theta_c + \sqrt{1 - \alpha/\alpha_c}/z$).

On the unlocked side, it is convenient to treat the discrete series $y_n = \theta_n - \theta_c$ as a continuous function $y(n)$, since near θ_c each iteration step changes θ only slightly ("staircase" diagram in Fig. 5). Then, from (C1) and (C4),

$$\frac{dy}{dn} = \alpha_c - \alpha - \alpha_c z^2 y^2. \tag{C5}$$

This equation can be easily integrated in order to determine how long it takes the phase to pass through the bottleneck (Fig. 4). For that, the limits of integration over y can be extended to the full real axis (details of the map function away

from θ_c do not matter in this regime, since it takes a much shorter time to go through regions other than the bottleneck).

Thus the estimate for the total number of drive periods for the phase to wind by 2π relative to the drive is

$$\begin{aligned} N(\alpha) &= \frac{1}{\alpha - \alpha_c} \int_{-\infty}^{\infty} \frac{dy}{1 + \frac{\alpha_c}{\alpha - \alpha_c} z^2 y^2} \\ &= \frac{\pi}{z\sqrt{\alpha_c |\alpha - \alpha_c|}}. \end{aligned}$$

This translates into the time period $T_{LC} = 2\pi N(\alpha)/\omega_d$ per 2π phase slip. Thus, the periodic oscillation of y gives rise to sideband spectral peaks split from the drive frequency by integer multiples of $2\pi/T_{LC} \propto \sqrt{|\alpha - \alpha_c|}$.

[1] A. N. Cleland and M. L. Roukes, Noise processes in nanomechanical resonators, J. Appl. Phys. **92**, 2758 (2002).

[2] E. Buks, S. Zaitsev, E. Segev, B. Abdo, and M. P. Blencowe, Displacement detection with a vibrating RF SQUID: Beating the standard linear limit, Phys. Rev. E **76**, 026217 (2007).

[3] D. Rugar, H. J. Mamin, and P. Guethner, Improved fiber-optic interferometer for atomic force microscopy, Appl. Phys. Lett. **55**, 2588 (1989).

[4] O. Arcizet, P. F. Cohadon, T. Briant, M. Pinard, A. Heidmann, J. M. Mackowski, C. Michel, L. Pinard, O. Francais, and L. Rousseau, High-Sensitivity Optical Monitoring of a Micromechanical Resonator with a Quantum-Limited Optomechanical Sensor, Phys. Rev. Lett. **97**, 133601 (2006).

[5] S. Forstner, S. Prams, J. Knittel, E. D. van Ooijen, J. D. Swaim, G. I. Harris, A. Szorkovszky, W. P. Bowen, and H. Rubinstein-Dunlop, Cavity Optomechanical Magnetometer, Phys. Rev. Lett. **108**, 120801 (2012).

[6] S. Stapfner, L. Ost, D. Hunger, J. Reichel, I. Favero, and E. M. Weig, Cavity-enhanced optical detection of carbon nanotube brownian motion, Appl. Phys. Lett. **102**, 151910 (2013).

[7] I. Baskin, D. Yuvaraj, G. Bachar, K. Shlomi, O. Shtempluck, and E. Buks, Optically induced self-excited oscillations in an on-fiber optomechanical cavity, J. Microelectromech. Syst. **23**, 563 (2014).

[8] V. Braginsky and A. Manukin, Ponderomotive effects of electromagnetic radiation, Sov. Phys. JETP **25**, 653 (1967).

[9] K. Hane and K. Suzuki, Self-excited vibration of a self-supporting thin film caused by laser irradiation, Sens. Actuators A **51**, 179 (1996).

[10] S. Gigan, H. R. Böhm, M. Paternostro, F. Blaser, J. B. Hertzberg, K. C. Schwab, D. Bauerle, M. Aspelmeyer, and A. Zeilinger, Self cooling of a micromirror by radiation pressure, Nature (London) **444**, 67 (2006).

[11] C. H. Metzger and K. Karrai, Cavity cooling of a microlever, Nature (London) **432**, 1002 (2004).

[12] T. J. Kippenberg and K. J. Vahala, Cavity optomechanics: Back-action at the mesoscale, Science **321**, 1172 (2008).

[13] C. M. I. Favero, S. Camerer, D. Konig, H. Lorenz, J. P. Kotthaus, and K. Karrai, Optical cooling of a micromirror of wavelength size, Appl. Phys. Lett. **90**, 104101 (2007).

[14] F. Marquardt and S. M. Girvin, Optomechanics, Physics **2**, 40 (2009).

[15] S. E. Lyshevski and M. Lyshevski, Nano- and microoptoelectromechanical systems and nanoscale active optics, in *Third IEEE Conference on Nanotechnology* (IEEE, Piscataway, NJ, 2003), pp. 840–843.

[16] N. Stokes, F. Fatah, and S. Venkatesh, Self-excited vibrations of optical microresonators, Electron. Lett. **24**, 777 (1988).

[17] M. Hossein-Zadeh and K. J. Vahala, An optomechanical oscillator on a silicon chip, IEEE J. Sel. Top. Quantum Electron. **16**, 276 (2010).

[18] M. C. Wu, O. Solgaard, and J. E. Ford, Optical MEMS for lightwave communication, J. Lightwave Technol. **24**, 4433 (2006).

[19] M. Eichenfield, C. P. Michael, R. Perahia, and O. Painter, Actuation of micro-optomechanical systems via cavity-enhanced optical dipole forces, Nat. Photon. **1**, 416 (2007).

[20] G. Bahl, J. Zehnpfennig, M. Tomes, and T. Carmon, Stimulated optomechanical excitation of surface acoustic waves in a microdevice, Nat. Commun. **2**, 403 (2011).

[21] N. Flowers-Jacobs, S. Hoch, J. Sankey, A. Kashkanova, A. Jayich, C. Deutsch, J. Reichel, and J. Harris, Fiber-cavity-based optomechanical device, Appl. Phys. Lett. **101**, 221109 (2012).

[22] M. Poot and H. S. van der Zant, Mechanical systems in the quantum regime, Phys. Rep. **511**, 273 (2012).

[23] T. J. Kippenberg, H. Rokhsari, T. Carmon, A. Scherer, and K. J. Vahala, Analysis of Radiation-Pressure Induced Mechanical Oscillation of an Optical Microcavity, Phys. Rev. Lett. **95**, 033901 (2005).

[24] H. Rokhsari, T. Kippenberg, T. Carmon, and K. Vahala, Radiation-pressure-driven micro-mechanical oscillator, Opt. Express **13**, 5293 (2005).

[25] O. Arcizet, P. F. Cohadon, T. Briant, M. Pinard, and A. Heidmann, Radiation-pressure cooling and optomechanical instability of a micromirror, Nature (London) **444**, 71 (2006).

[26] D. Kleckner and D. Bouwmeester, Sub-kelvin optical cooling of a micromechanical resonator, Nature (London) **444**, 75 (2006).

[27] G. Jourdan, F. Comin, and J. Chevrier, Mechanical Mode Dependence of Bolometric Backaction in an Atomic Force Microscopy Microlever, Phys. Rev. Lett. **101**, 133904 (2008).

[28] F. Marino and F. Marin, Chaotically spiking attractors in suspended-mirror optical cavities, Phys. Rev. E **83**, 015202(R) (2011).

[29] C. Metzger, M. Ludwig, C. Neuenhahn, A. Ortlieb, I. Favero, K. Karrai, and F. Marquardt, Self-Induced Oscillations in an Op-

tomechanical System Driven by Bolometric Backaction, Phys. Rev. Lett. **101**, 133903 (2008).

[30] J. Restrepo, J. Gabelli, C. Ciuti, and I. Favero, Classical and quantum theory of photothermal cavity cooling of a mechanical oscillator, C. R. Phys. **12**, 860 (2011).

[31] S. D. Liberato, N. Lambert, and F. Nori, Quantum limit of photothermal cooling, Phys. Rev. A **83**, 033809 (2011).

[32] F. Marquardt, J. G. E. Harris, and S. M. Girvin, Dynamical Multistability Induced by Radiation Pressure in High-Finesse Micromechanical Optical Cavities, Phys. Rev. Lett. **96**, 103901 (2006).

[33] M. Paternostro, S. Gigan, M. S. Kim, F. Blaser, H. R. Böhm, and M. Aspelmeyer, Reconstructing the dynamics of a movable mirror in a detuned optical cavity, New J. Phys. **8**, 107 (2006).

[34] D. Yuvaraj, M. B. Kadam, O. Shtempluck, and E. Buks, Optomechanical cavity with a buckled mirror, J. Microelectromech. Syst. **22**, 430 (2013).

[35] K. Aubin, M. Zalalutdinov, T. Alan, R. Reichenbach, R. Rand, A. Zehnder, J. Parpia, and H. Craighead, Limit cycle oscillations in CW laser-driven NEMS, J. Microelectromech. Syst. **13**, 1018 (2004).

[36] S. Zaitsev, A. K. Pandey, O. Shtempluck, and E. Buks, Forced and self-excited oscillations of optomechanical cavity, Phys. Rev. E **84**, 046605 (2011).

[37] S. Zaitsev, O. Gottlieb, and E. Buks, Nonlinear dynamics of a microelectromechanical mirror in an optical resonance cavity, Nonlin. Dyn. **69**, 1589 (2012).

[38] K. Kim and S. Lee, Self-oscillation mode induced in an atomic force microscope cantilever, J. Appl. Phys. **91**, 4715 (2002).

[39] T. Carmon, H. Rokhsari, L. Yang, T. J. Kippenberg, and K. J. Vahala, Temporal Behavior of Radiation-Pressure-Induced Vibrations of an Optical Microcavity Phonon Mode, Phys. Rev. Lett. **94**, 223902 (2005).

[40] T. Corbitt, D. Ottaway, E. Innerhofer, J. Pelc, and N. Mavalvala, Measurement of radiation-pressure-induced optomechanical dynamics in a suspended fabry-perot cavity, Phys. Rev. A **74**, 021802(R) (2006).

[41] T. Carmon and K. J. Vahala, Modal Spectroscopy of Optoexcited Vibrations of a Micron-Scale On-Chip Resonator at Greater Than 1 GHZ Frequency, Phys. Rev. Lett. **98**, 123901 (2007).

[42] K. Shlomi, D. Yuvaraj, I. Baskin, O. Suchoi, R. Winik, and E. Buks, Synchronization in an optomechanical cavity, Phys. Rev. E **91**, 032910 (2015).

[43] H. Wang, Y. Dhayalan, and E. Buks, Devil's staircase in an optomechanical cavity, Phys. Rev. E **93**, 023007 (2016).

[44] M. Zhang, G. S. Wiederhecker, S. Manipatruni, A. Barnard, P. McEuen, and M. Lipson, Synchronization of Micromechanical Oscillators Using Light, Phys. Rev. Lett. **109**, 233906 (2012).

[45] M. Bagheri, M. Poot, L. Fan, F. Marquardt, and H. X. Tang, Photonic Cavity Synchronization of Nanomechanical Oscillators, Phys. Rev. Lett. **111**, 213902 (2013).

[46] Y. Dhayalan, I. Baskin, K. Shlomi, and E. Buks, Phase Space Distribution Near the Self-Excited Oscillation Threshold, Phys. Rev. Lett. **112**, 210403 (2014).

[47] D. Anderson, V. Mizrahi, T. Erdogan, and A. White, Production of in-fibre gratings using a diffractive optical element, Electron. Lett. **29**, 566 (1993).

[48] A. K. Pandey, O. Gottlieb, O. Shtempluck, and E. Buks, Performance of an AuPd micromechanical resonator as a temperature sensor, Appl. Phys. Lett. **96**, 203105 (2010).

[49] V. S. Anishchenko and T. E. Vadivasova, Synchronization of self-oscillations and noise-induced oscillations, J. Commun. Technol. Electron. **47**, 117 (2002).

[50] M. Pandey, R. H. Rand, and A. T. Zehnder, Frequency locking in a forced Mathieu–van der Pol–Duffing system, Nonlin. Dyn. **54**, 3 (2008).

[51] L. Paciorek, Injection locking of oscillators, Proc. IEEE **53**, 1723 (196).

[52] R. Adler, A study of locking phenomena in oscillators, Proc. IRE **34**, 351 (1946).

[53] M. H. Jensen, P. Bak, and T. Bohr, Complete Devil's Staircase, Fractal Dimension, and Universality of Mode-Locking Structure in the Circle Map, Phys. Rev. Lett. **50**, 1637 (1983).

[54] S. Dos Santos and M. Planat, Generation of 1/f noise in locked systems working in nonlinear mode, IEEE Trans. Ultrason. Ferroelectr. Freq. Contr. **47**, 1147 (2000).

[55] R. Hamerly and H. Mabuchi, Optical Devices Based on Limit Cycles and Amplification in Semiconductor Optical Cavities, Phys. Rev. Appl. **4**, 024016 (2015).

[56] C. Huygens and H. Oscillatorium, The pendulum clock, *Trans RJ Blackwell* (The Iowa State University Press, Ames, IA, 1986).

[57] M. Rosenblum and A. Pikovsky, Synchronization: From pendulum clocks to chaotic lasers and chemical oscillators, Contemp. Phys. **44**, 401 (2003).

[58] G. Heinrich, M. Ludwig, J. Qian, B. Kubala, and F. Marquardt, Collective Dynamics in Optomechanical Arrays, Phys. Rev. Lett. **107**, 043603 (2011).

[59] M. Dykman, X. Chu, and J. Ross, Stationary probability distribution near stable limit cycles far from Hopf bifurcation points, Phys. Rev. E **48**, 1646 (1993).

[60] H. Risken, *The Fokker-Planck Equation: Methods of Solution and Applications* (Springer, 1996).

[61] K. Y. Fong, M. Poot, X. Han, and H. X. Tang, Phase noise of self-sustained optomechanical oscillators, Phys. Rev. A **90**, 023825 (2014).

[62] M. Tinkham, *Introduction to Superconductivity* (Krieger, Florida, 1975).

[63] S. Kogan, *Electronic Noise and Fluctuations in Solids* (Cambridge University Press, Cambridge, 2008).

[64] Y. Levinson, Quantum noise in a current-biased Josephson junction, Phys. Rev. B **67**, 184504 (2003).

[65] S. Strogatz, *Nonlinear Dynamics and Chaos: With Applications to Physics, Biology, Chemistry and Engineering* (Perseus Books Group, 2000).

[66] H. A. Kramers, Brownian motion in a field of force and the diffusion model of chemical reactions, Physica **7**, 284 (1940).

[67] P. Hanggi, P. Talkner, and M. Borkovec, Reaction-rate theory: Fifty years after Kramers, Rev. Mod. Phys. **62**, 251 (1990).

[68] S. Zaitsev, O. Shtempluck, E. Buks, and O. Gottlieb, Nonlinear damping in a micromechanical oscillator, Nonlin. Dyn. **67**, 859 (2012).

[69] R. D. Hempstead and M. Lax, Classical noise. vi. noise in self-sustained oscillators near threshold, Phys. Rev. **161**, 350 (1967).

[70] E. Ben-Jacob, Y. Braiman, R. Shainsky, and Y. Imry, Microwave-induced devil's staircase structure and chaotic be-havior in current-fed josephson junctions, Appl. Phys. Lett. **38**, 822 (1981).

[71] C. Reichhardt and F. Nori, Phase Locking, Devil's Staircases, Farey Trees, and Arnold Tongues in Driven Vortex Lattices with Periodic Pinning, Phys. Rev. Lett. **82**, 414 (1999).

[72] S.-B. Shim, M. Imboden, and P. Mohanty, Synchronized oscil-lation in coupled nanomechanical oscillators, Science **316**, 95 (2007).